Steel and Composite Structures, Vol. 13, No. 4 (2012) 383-396
DOI: http://dx.doi.org/10.12989/scs.2012.13.4.383

Experimental study on ductile crack initiation in compact section steel columns

Xiaoqun Luo[1,2], Hanbin Ge*[3] and Masatoshi Ohashi[4]

[1]*Associate Professor, Dept. of Building Engineering, Tongji University, Shanghai 200092, P.R.China*
[2]*Former Post Doctoral Researcher, Dept. of Civil Engineering, Meijo University, Nagoya 468-8502, Japan*
[3]*Professor, Dept. of Civil Engineering, Meijo University, Nagoya 468-8502, Japan*
[4]*Central Japan Railway Company, Nagoya 450-6101, Japan*

(Received October 21, 2009, Revised August 01, 2012, Accepted August 06, 2012)

Abstract. In order to develop a verification method for extremely low cycle fatigue (ELCF) of steel structures, the initiation mechanism of ductile cracks is investigated in the present study, which is the first step of brittle fracture, occurred in steel bridge piers with thick-walled sections. For this purpose, a total of six steel columns with small width-thickness ratios were tested under cyclic loading. It is found that ductile cracks occurred at the column base in all the specimens regardless of cyclic loading histories subjected. Moreover, strain history near the crack initiation location is illustrated and an index of energy dissipation amount is proposed to evaluate deformation capacity of structures.

Keywords: ductile crack initiation; brittle fracture; steel bridge; cyclic loading.

1. Introduction

In the 1995 Hyogoken-Nanbu earthquake, brittle fractures were observed in the corners of steel portal piers (Fig. 1). Because no similar damages ever being reported in Japan before, brittle fracture was not considered in seismic design prior to this earthquake. However, since then the necessity to account for brittle fracture in the phase of seismic design has been gradually realized. Thin-walled cross sections used to be frequently employed in civil engineering structures in Japan, and therefore local buckling was the principle failure mode of steel structures subjected to large low-cycle cyclic loads such as earthquake effects. After the Hyogoken-Nanbu earthquake, however, thick-walled cross sections become more favored for the purpose to improve deformation capacity of structures. As a consequence, brittle fracture resulting from ductile crack, which occurs prior to local buckling, becomes a possible failure mode of structures (JSCE 2000).

So far, most of researches regarding brittle fracture deal with development of high fracture ductility steels to prevent brittle fracture from material level, simulation of ductile crack initiation, and proposals of structure configurations free of strain concentration. As an instance of researches about steel materials, Divsalar *et al.* (1988) conducted low cycle fatigue (LCF) tests on rolled plates made of B.S. 4360-50D to investigate LCF behavior and a series of parameters was proposed to construct cyclic stress-

* Corresponding author, Ph.D., E-mail: gehanbin@meijo-u.ac.jp

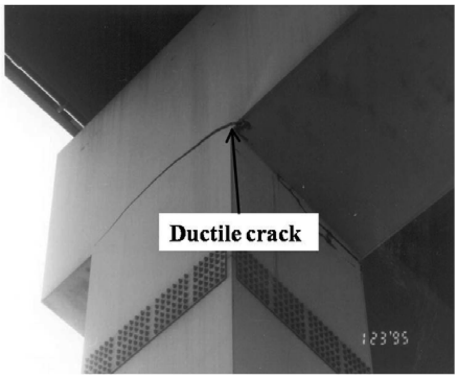

Fig. 1 Ductile fracture in steel bridge piers in the 1995 Kobe earthquake

strain relationship based on the Manson-Coffin law. In relatively recent research, Kuwamura (1997) revealed transitional cracking behavior between fatigue and ductile fracture in steels under cyclic testing. More analyses and experiments, including monotonic and cyclic tests for materials, standard fracture tests, smooth notched tests, pull plate tests, etc., were carried out on different varieties of steel and configurations of specimens, and steel type based distinctions existed in the features of LCF were further clarified (Li *et al.* 1998, Liu *et al.* 2005a, Liu *et al.* 2005b, Dusicka *et al.* 2007). Most of them employed the empirical equation of the Coffin-Manson law. Besides LCF research at material level, some investigations were conducted on structural components and systems under seismically cyclic loadings. Krawinkler and Zohrei (1983) proposed cumulative damage models to predict fatigue life for earthquake ground motions at weldment. Sakano and Wahab (2001) investigated the ELCF behavior of both steel pier beam-column joints and column based joints. Uriz and Mahin (2008) conducted large scale tests on brace components and concentrically frame systems to develop, calibrate and validate improved numerical models capable of simulating the behavior of braced frames, including possible failure due to local buckling and ELCF. In particular, the effectiveness of Manson-Coffin law was verified in respect of the relationship between the crack initiation life and the range of local plastic strains at the location of crack initiation at beam-column joints or column bases. In addition, there is research on proposals of structure configurations free of strain concentration. Ductile web fracture initiation in steel shear links was observed through a quasi-static cyclic loading test, and numerical simulations were performed to modify existing judging criterion and accordingly alternative stiffener configurations were recommended (McDaniel *et al.* 2003, Chao *et al.* 2006).

When a structure is subjected to large cyclic loads, strains tend to concentrate in regions with geometric discontinuity such as beam-column joint corners and column bases. If the concentrated strains continue to increase and exceed the ductile limitations of the material, ductile crack initiates. With additional cyclic loads applied, ductile crack transforms to brittle crack, which eventually leads the structure to brittle fracture (Ge *et al.* 2007). Based on the basic design conception to prevent brittle fracture by avoiding small cracks, the present study focuses on ductile crack initiation, which is the first phase of brittle fracture, and tries to clarify its mechanism. The objective of the study is to provide necessary data for the development of verification method for ELCF of steel structures. To this end, cyclic loading experiment is conducted on high ductility steel piers made of thick-walled cross sections to investigate ductile crack initiation and its propagation.

2. Experimental specimens and loading arrangement

The tested specimens are unstiffened steel columns with square box section as shown in Fig. 2. In order to simulate brittle fracture behavior which initiates from ductile cracks, thick-walled cross sections with width-to-thickness ratio parameter R_f of 0.25 and 0.35, for which local buckling is not likely to occur, are employed. Slenderness ratio parameter $\bar{\lambda}$ is chosen to be 0.25 and 0.35. R_f and $\bar{\lambda}$ are defined by the following equations.

$$R_f = \frac{b}{t}\sqrt{\frac{\sigma_y}{E}\cdot\frac{12(1-\nu^2)}{4\pi^2}} \tag{1}$$

$$\bar{\lambda} = \frac{2h}{r}\frac{1}{\pi}\sqrt{\frac{\sigma_y}{E}} \tag{2}$$

where, b, t and r are the width, thickness and radius of gyration of cross section, respectively; h is the column height; σ_y is the yield stress; E and ν are Young's modulus and Poisson's ratio, respectively. The dimensions measured from the specimens are listed in Table 1, where B is the width of flange; D is

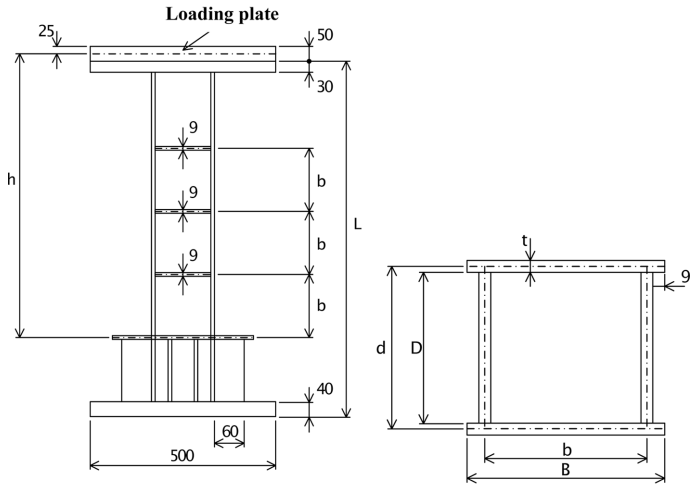

(a) Elevated view (Unit: mm) (b) Plan View (Unit: mm)

Fig. 2 Test specimen

Table 1 Dimensions and parameters of test specimens

Specimen	B (mm)	D (mm)	b (mm)	d (mm)	t (mm)	L (mm)	h (mm)	R_f	$\bar{\lambda}$	δ_y (mm)	H_y (kN)	P/P_y
UB25-25C1P1	152.4	114.9	124.9	124.7	9.17	756	552	0.25	0.24	2.02	82.28	0.1
UB25-25C3P1	152.4	114.9	125.1	124.0	9.11	755	551	0.25	0.23	2.01	81.71	0.1
UB35-25C1	202.3	165.0	174.1	174.3	9.33	956	772	0.34	0.24	3.12	127.67	0.0
UB35-25M	202.3	164.0	174.3	173.3	9.34	954	770	0.34	0.24	3.10	126.55	0.0
UB25-35C1	152.6	114.8	125.0	123.2	9.19	955	771	0.25	0.33	4.08	65.50	0.0
UB25-35C3	152.2	114.6	124.6	123.8	9.20	955	771	0.25	0.33	4.09	65.43	0.0

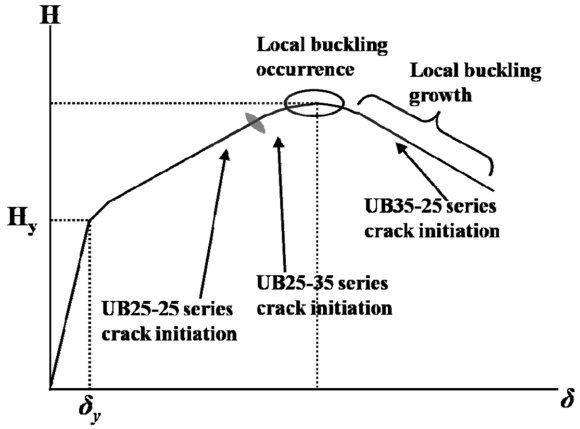

Fig. 3 Failure mode prediction in test specimens

the depth of web; and L is the height of specimens.

Failure mode prediction for tested specimens is shown in Fig. 3, which exhibits the possible failure relationship between ductile crack initiation and local buckling. Among the three series of specimens, local buckling would occur prior to ductile crack initiation in the UB35-25 series which has the thinnest cross section because of relatively large R_f. While in the other two series, ductile crack would initiate first.

Notation of a specimen such as UB00-XXC1P1 is explained as follows. UB means unstiffened box section, 00 refers to the two numerals after decimal point of R_f, and XX refers to that of $\bar{\lambda}$, C indicates cyclic loading and P indicates axial force. C1 refers to cyclic loading with varying amplitude, and 1 cycle at each amplitude, whereas C3 means 3 cycles repeated at each amplitude. M refers to monotonic loading. SM400A steel for welded structures is used for the specimens. Results obtained from material tension test are shown in Table 2. Calculated R_f and $\bar{\lambda}$ according to the material properties are shown in Table 1. Flanges and webs are welded by groove welding on both sides. It is noted that the flanges are welded with an extension part 9 mm long.

As shown in Fig. 2, the specimen is fixed at the bottom. In the vertical direction, conventionally, a constant axial compression force is applied at the top of the specimen. Since it is known that cracks are induced by tension force, in order to make sure cracks will initiate, in addition to the conventional loading cases with axial compression force, loadings without axial force are conducted in two cases. In the lateral direction, displacement controlled horizontal loads are applied at the top of the specimen. Loading patterns include monotonic loading, one-cycle reversal and three-cycle reversal cyclic loading as shown in Fig. 4. For the one-cycle reversal loading shown in Fig. 4(b), the amplitude is progressively increased with an increment of $1\delta_y$ per each cycle. However, in the cases that a crack initiates prior to $10\delta_y$, the amplitude will be increased with an increment of $2\delta_y$ per each cycle in the subsequent loading. For the three-cycle reversal loading shown in Fig. 4(c), the amplitude is increased in the sequence of $\delta/\delta_y = 3, 6, 9$, *et al.*, and 3 cycles of load are repeated at each amplitude. Here δ_y refers to the horizontal

Table 2 Material properties

E (GPa)	ν	E_{st} (GPa)	σ_y (MPa)	ε_y (%)	ε_{st} (%)	σ_u (MPa)	ε_u (%)
202	0.29	3.66	241	0.12	1.3	387	33

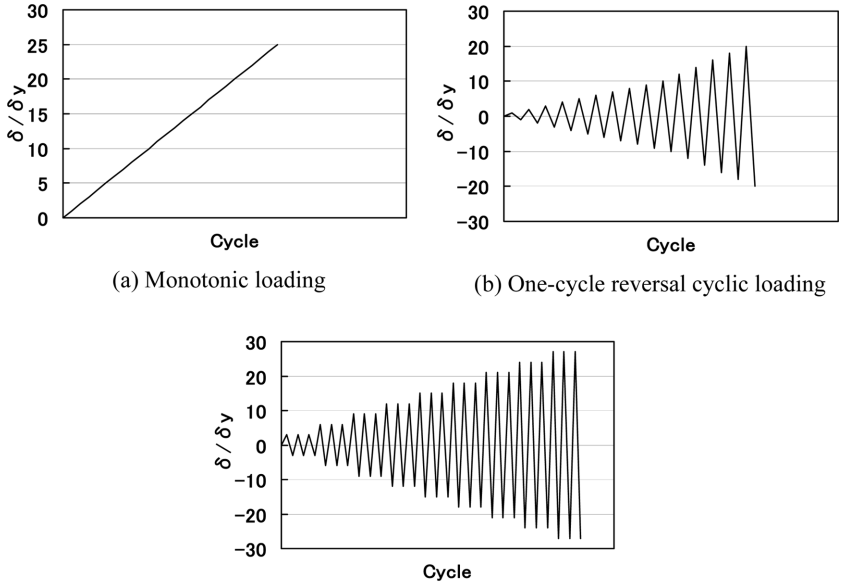

(a) Monotonic loading

(b) One-cycle reversal cyclic loading

(c) Three-cycle reversal cyclic loading

Fig. 4 Loading patterns

displacement at the top of the specimen when the flange at the bottom first yields.

As crack initiation is expected to occur near the ends of welding at the bottom of the specimen, strain gauges are attached at locations 10 mm above the welding of the flange and pier base plate, and locations on the flange 10 mm horizontally away from the welding of the flange and web, to measure the strains near crack initiation location.

Tests are terminated when load falls below 50% of its maximum value, or a crack reaches half length of the flange.

3. Experimental results

3.1 Definition of ductile crack initiation point

One of the most important factors in the present experiment is to define crack initiation. Crack initiation is defined as the point when crack length extends to 1-2 mm according to visual and photographic observations. As will be explained later, initial propagation of crack is not abrupt and will not immediately lead to brittle fracture, this definition does not result in a dangerous evaluation.

Definition of ductile crack initiation point in this experiment is explained as follows. Shown in Fig. 5 is the image of a load-displacement curve (envelope curve) obtained from the experiment. In the case that crack initiation is confirmed on the loading loop from $-4\delta_y$ to $+5\delta_y$ (the point indicated by ◎), the ductile crack initiation point is defined as the previous load reversal point which is $+4\delta_y$. This definition is made conservative purposely to counteract the roughness in determination of crack initiation which is based on visual observation. Similarly, in the case that crack initiation is confirmed on the loop from $+4\delta_y$ to $-4\delta_y$ (the point indicated by ▲), $-3\delta_y$ is considered as the ductile crack initiation point.

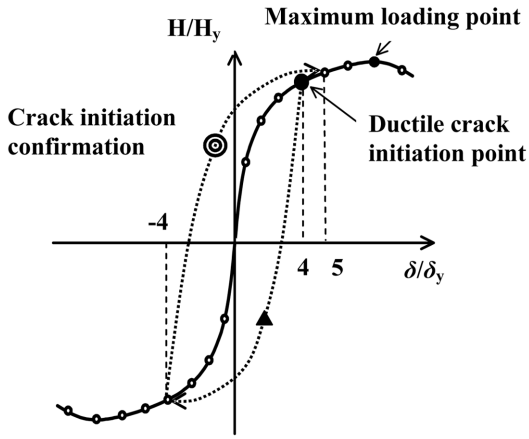

Fig. 5 Definition of ductile crack initiation point

3.2 Load-displacement relations

Shown in Fig. 6 are the hysteretic curves of horizontal load versus horizontal displacement obtained from cyclic loading tests of four specimens with R_f = 0.25. Horizontal load and horizontal displacement are divided by H_y and δ_y respectively to be dimensionless. Values of H_y and δ_y are shown in Table 1. As can be seen from the graph, due to use of thick-walled cross sections, an evident cyclic strain hardening effect at work can be found with the continuous increase of load as cycling progresses. In the test, deformations resulting from local buckling were observed in specimens with relatively small width-to-thickness ratio (R_f = 0.25), however, these deformations were very hard to be detected by eyes here but the sense of touch by hand and it hardly grew even when the amplitude of displacement controlled cyclic loading was enlarged. In contrast to this, ductile cracks that initiated prior to local buckling continued to grow larger gradually, and upon its length reaching to a certain value, a sudden drop of strength occurred. On the other hand, in the cases of specimens with R_f = 0.35, though slight local buckling proceeded crack initiation, it ceased to develop in spite of continued cycling. Eventually these specimens lost strength capacity due to initiation and propagation of crack at the base just the same as other specimens.

Fig. 6(e) shows the hysteretic curve of specimen UB35-25M in a monotonic loading test. Since no crack initiation was confirmed until the displacement controlled loading was increased to nearly loading capacity limit, the loading was reversed with constant amplitude. As a consequence, when the loading was reversed for the first time crack initiated at the base on the side that was at first compressed, and the crack suddenly started to grow rapidly in the next loading cycle, which greatly reduced the strength of the specimen.

Envelope curves of the hysteretic horizontal load-horizontal deflection relations of all four specimens are shown in Fig. 7. In the two tests of UB25-25C3P1 and UB25-35C3 that are subjected to three-cycle reversal loading, it is noted that the envelope curves are drawn at the third cycle of each amplitude. The ductile crack initiation points obtained according to the definition shown in Fig. 5 are indicated by ●. From the figures, it is understood that strength is still increasing due to cyclic strain hardening when ductile crack occurs. For the two specimens UB25-25C3P1 and UB25-25C1P1 that are loaded with axial compression force, the ductile crack initiations occur at around $10\delta_y$, whereas ductile crack

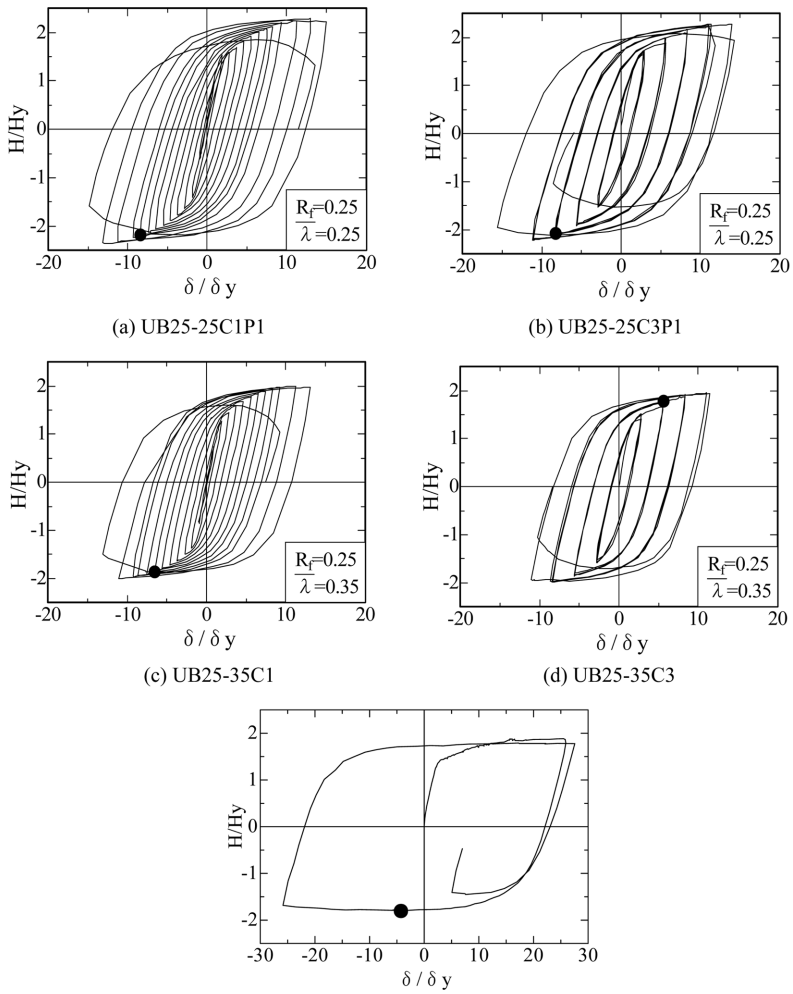

Fig. 6 Lateral load-displacement hysteretic curve

initiation points of the two specimens without axial compression force UB25-35C1 and UB25-35C3 are approximately 6 or 7δ_y. It is indicated that the deformation capacity in the specimens without axial compression force is lower than that in the ones with axial compression force. However, when parameters of the models are compared, it is worth noting that their slenderness ratio parameters are different. Though slightly affected by distinctions of structural and loading parameters, it is found in the load-displacement curves that the reduction of strength generally does not occur in the subsequent 3-5 cycles following crack initiation.

Horizontal displacements $\delta_{u,c}$ and δ_{max}, which correspond to ductile crack initiation point defined in the present study and the maximum loading point, respectively, are shown in Table 3. They are nondimensionalized by the horizontal yield displacement δ_y. According to Table 3, δ_{max}/δ_y is larger than

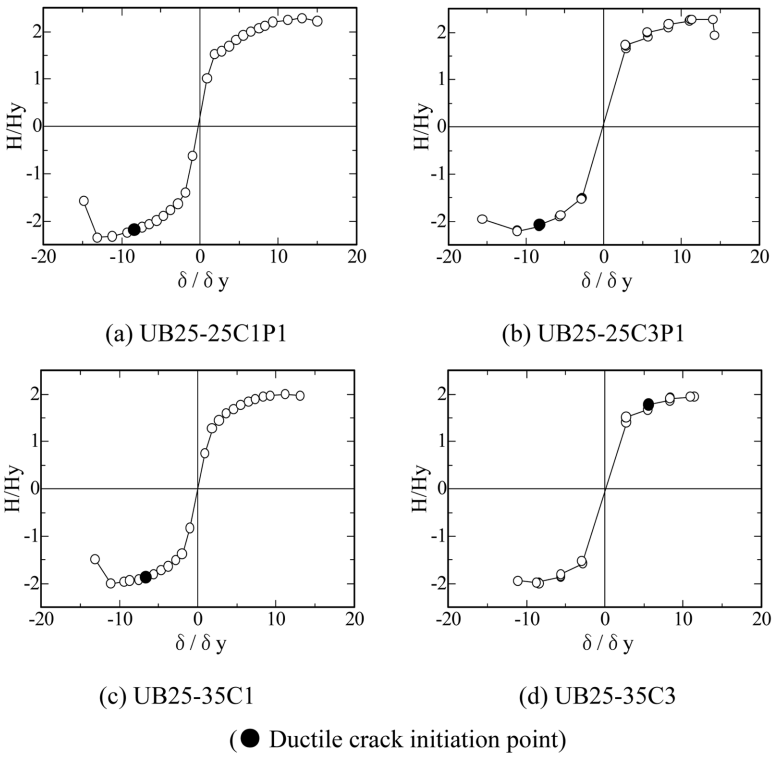

Fig. 7 Envelope curve of load-displacement relationship and ductile crack initiation point

Table 3 Lateral displacements corresponding to ductile crack initiation and maximum load points as well as strains at ductile crack initiation points

Specimen	$\frac{\delta_{u,c}}{\delta_y}$	$\frac{\delta_{max}}{\delta_y}$	$\frac{\delta_{u,c}}{\delta_{max}}$	$\varepsilon_{u,c}$	ε_{eff}^{p} (%)	When crack occurs?
UB25-25C1P1	9	14	0.64	0.011	3.55	From $10\delta_y$ to $-10\delta_y$
UB25-25C3P1	9	15	0.60	0.016	4.66	Towards $-9\delta_y$ (2nd cycle)
UB35-25C1	10	13	0.77	0.036	4.73	At reversal point of $10\delta_y$
UB25-35C1	7	12	0.58	0.031	5.11	From $8\delta_y$ to $-8\delta_y$
UB25-35C3	6	12	0.50	0.025	3.56	From $-6\delta_y$ (3rd cycle) to $9\delta_y$

$\delta_{u,c}/\delta_y$ because the load still increases even after reaching the ductile crack initiation point. In addition, the ductile crack initiation point to maximum load point displacement ratio ($\delta_{u,c}/\delta_{max}$) is approximately 0.6 with an exception of case UB35-25C1. It is understood that ductile crack will grow with certain stability instead of immediately leading to brittle fracture after its initiation.

3.3 Crack Initiation and propagation

Taking the test of UB25-35C1 as example, ductile crack propagation is illustrated in Fig. 8. The

situation when yield displacement is up to for the first time is shown in Fig. 8(a). As shown in Fig. 8(b), on the loading loop from $8\delta_y$ to $9\delta_y$, crack initiation was observed at the extension part of the flange of the column base while local buckling did not appear at this moment. According to the definition of ductile crack initiation point, $-7\delta_y$ is considered as the ductile crack initiation point shown in Fig. 6(c) and Fig. 7(c). In the subsequent three cycles, the crack did not grow with evident growth after its initiation. Because of the influence of strain hardening, it is found in the load-displacement relation shown in Fig. 6(c) and the envelope curve shown in Fig. 7(c) that the loading increased slowly after ductile crack initiated. When the load was about to reach to its maximum value of $12\delta_y$ as shown in Fig. 8(c), slight local buckling deformation was observed. Meanwhile, the crack was extending through the flange thickness, as well as along the welding lines on both sides. The following crack propagation is illustrated as solid line in Fig. 8(f). After having extended for about 10 mm along the welding lines, the crack starts penetrating into base metal. As shown in Fig. 8(d), around $14\delta_y$, the crack started to propagate into base metal which triggered decrease of strength capacity. As shown in Fig. 8(e), in the following cyclic loop towards $-14\delta_y$, the crack grew rapidly. And when the crack length exceeded 20 mm, the strength capacity reduced remarkably. Crack initiation at the identical locations and similar crack propagation were also witnessed in other specimens.

Illustration of crack propagation is shown in Fig. 9(a), with horizontal and vertical axes representing crack length and horizontal load respectively. Here crack length indicates length along the flange edge measured at displacement reversal points. As evidenced by all the models, load keeps almost constant without deterioration or increases continuously due to cyclic strain hardening even after ductile crack initiation point. The strength capacity begins to decrease when crack length reaches approximately 20 mm, though this value varies slightly with respect to structural and loading parameters. Shown in Fig. 9(b) is the illustration of crack length at the extension part of flange, from which it can be seen that the sum of length of flange extension and web thickness is equal to 18 mm. Therefore crack length of 20 mm indicates penetration of crack into the base metal. It can be further understood that the strength does not decrease when crack initiates at the welding end, or propagates through plate thickness and

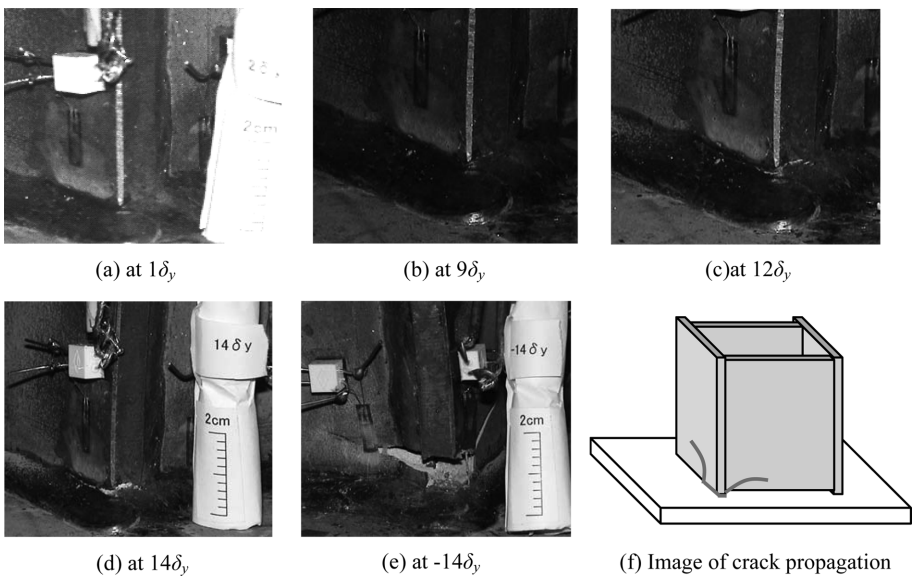

(a) at $1\delta_y$ (b) at $9\delta_y$ (c)at $12\delta_y$

(d) at $14\delta_y$ (e) at $-14\delta_y$ (f) Image of crack propagation

Fig. 8 Ductile crack initiation and propagation (UB25-35C1)

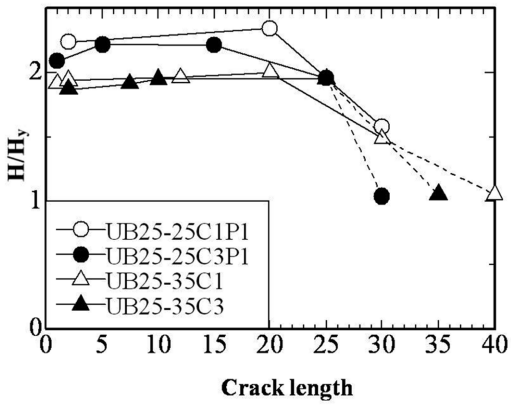

(a) Crack length-load capacity relations

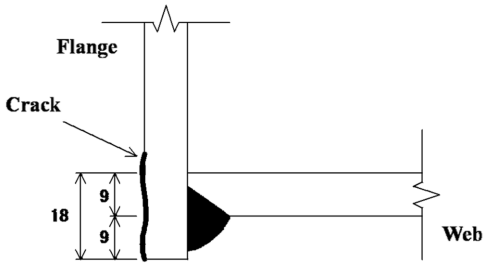

(b) Crack propagation at extension part

Fig. 9 Crack propagation and load capacity relations

along welding lines. Indeed, sudden drop of strength occurs only after crack extends to the base metal.

3.4 Strain history

Strain gauges were attached at 10 mm height to the weld of flange and base plate and 10 mm horizontally away from the edge of flange in the direction of flange. History of strains measured by the

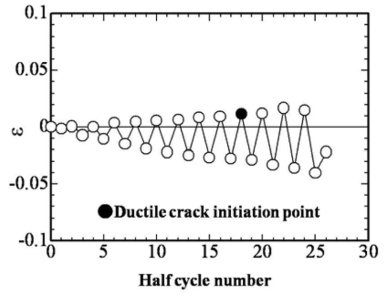

(a) UB25-25C1P1

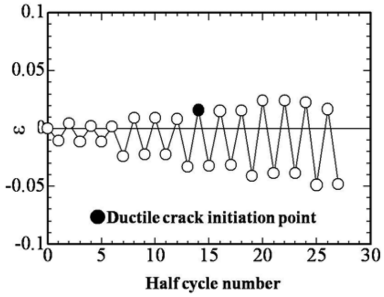

(b) UB25-25C3P1

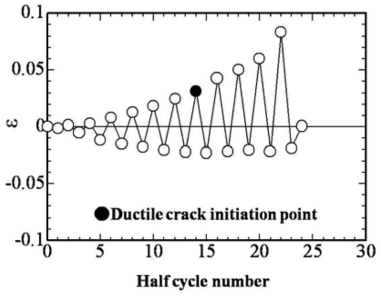

(c) UB25-35C1

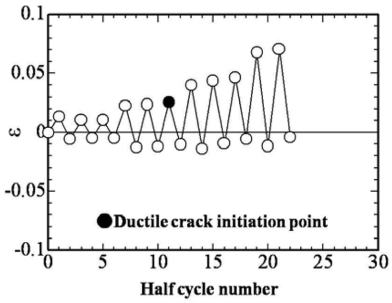

(d) UB25-35C3

Fig. 10 Strain progress near ductile crack locations

strain gauge is illustrated in Fig. 10. Horizontal and vertical axes refer to number of half cycles and strain respectively. Ductile crack initiation point is indicated by ●. The comparison of strain histories between specimen series shows that tensile strain gradually increases in UB25-25 series, whereas in UB25-35 series, a different progress with large increase of tensile strain is observed. This distinction arises from the application of axial compression force. In UB25-35 series due to the absence of axial compression force, tensile strains are able to develop as a result of cyclic loading. In addition, due to the distinction of slenderness ratio parameter, influence of P-δ effect can not be excluded either.

Strains at ductile crack initiation point are shown in Table 3. In the cases with axial compression force in UB25-25 series, the strains are approximately over 1%, whereas in cases without axial compression force, they are about 2.5-3.1%. However, since stain gauges are attached about 10 mm away from crack initiation locations, the strains at crack initiation locations should be even larger because of strain concentration. Comparison between cases of specimens under one-cycle reversal loading and three-cycle reversal loading shows no evident distinction in the present experiment. It is also demonstrated that crack initiation was confirmed after approximately the same number of loading cycles.

Finally, effective plastic strains are also summarized, according to the definition shown in Fig. 11 and the measurements of strain gauges attached at the base of specimens. The results are listed in Table 3, from which it is known the effective plastic strains are in the range of 7.5 -12% despite slight variations.

4. Energy dissipation

Energy dissipation amount is an index to evaluate deformation capacity of structures. As an important index in seismic performance assessment, energy dissipation amount indicates how much a structure can dissipate seismic energy during an earthquake. Definition of energy dissipation amount is shown in Fig. 12. Relations of cumulative energy dissipation versus half cycle numbers obtained from load-displacement curves are shown in Fig. 13. The energy dissipation amount is divided by $E_0 = H_y\delta_y/2$ to be dimensionless. As is aforementioned, ductile crack initiation point is $\delta/\delta_y = 9$ (9th cycle) for UB25-25C3P1 and UB25-25C1P1, $\delta/\delta_y = 7$ (7th cycle) for UB25-35C1, $\delta/\delta_y = 6$ (6th cycle) for UB25-35C3, as indicated by black solid marks in the figure. When cumulative energy dissipation under one-cycle reversal loading is compared, the value of $\Sigma E_i/E_0$ is approximately 300 in UB25-25 series with axial compression force and only 150 in UB25-35 series without axial compression force, which means ductile crack initiates when $\Sigma E_i/E_0$ exceeds 300 for UB25-25 series, and 150 for UB25-35 series. This

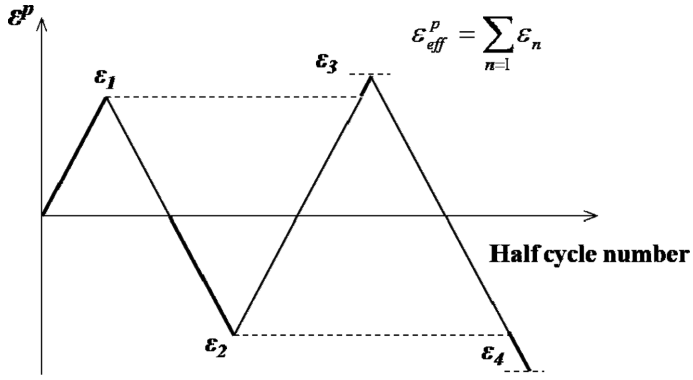

Fig. 11 Definition of effective plastic strain

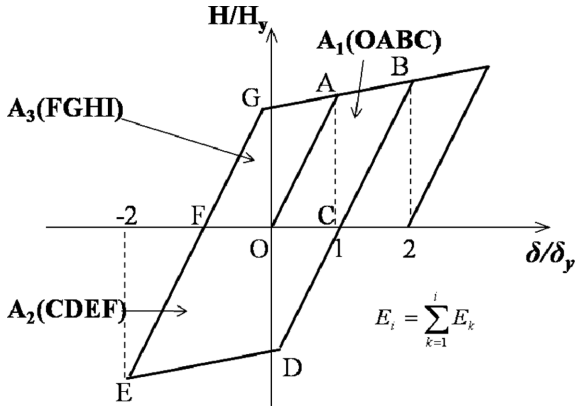

Fig. 12 Definition of energy dissipation

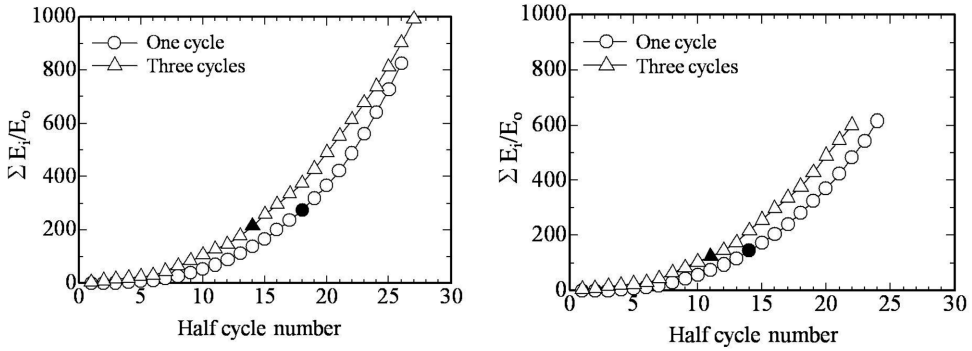

Fig. 13 Cumulative energy dissipation

fact indicates that in addition to structural parameters, the presence of axial compression force also has a significant influence on energy dissipation amount at crack initiation.

On the other hand, the distinction of cumulative energy dissipation between different loading patterns is also shown in Fig. 13. It is found that a little more energy is dissipated at ductile crack initiation point in three-cycle reversal loading than that in one-cycle reversal loading. Quantitative evaluation on the distinction should be performed in the future based on more experimental data.

5. Conclusions

In the present research, cyclic loading experiment is conducted on high deformation capacity steel piers made of thick-walled cross sections, ductile crack initiation and propagation are investigated and the following conclusions are obtained.

1) Crack initiation at the base is experimentally reproduced for all specimens.

2) Ductile crack initiates at the end of welding surface between flange and rib plate at the base of the specimen, with strength still increasing due to cyclic strain hardening.

3) Though additional loading results in crack propagation through flange thickness and along welding lines, immediate drop of strength does not occur. Upon penetration of crack into the base metal strength suddenly starts dropping rapidly.

4) Disregarding structural parameters and presence of axial compression force, crack penetrates into the base metal when crack length exceeds 20 mm, which leads to sudden drop of strength. However, this phenomenon is considered to be related to the length of flange extension part.

5) When crack initiates, measurement by strain gauges located 10 mm away from the crack indicates value of 1.1-3.5%, and effective plastic strain ranging from 7.5-12%. However, the real strain at the crack should be larger than the measured value due to strain concentration.

(6) When compared by cumulative energy dissipation index, at the ductile crack point, more energy is dissipated in UB25-25 series under compression than in UB25-35 series without compression, and more energy is dissipated under multi-cycle reversal loadings.

As the first step of developing verification method for ELCF of steel structures in seismic design, the initiation mechanism of ductile cracks is investigated in steel bridge piers with thick-walled sections. To more agree with actual situation, ELCF tests of steel bridge piers under random cyclic loadings should be conducted to simulate real earthquake. The behavior of different section configurations and different steel types need to be studied. Moreover, high performance analytical method considering weld imperfection should be developed to numerically simulate ELCF of steel structures.

Acknowledgements

The study was partially funded by grants from 1) Japan Science and Technology Agency for "Evaluation and Mitigation of Environment Impacts of Earthquake and Typhoon Disaster on Urban Area and Infrastructures" (Project Title: Refined Analysis and Damage Control of Earthquake Disaster Impact on Bridge Structures), under the Strategic Japanese-Chinese Cooperative Program on Science and Technology (S&T) for Environmental Conservation and Construction of a Society with Less Environmental Burden; and 2) the Advanced Research Center for Natural Disaster Risk Reduction, Meijo University, which is supported by Ministry of Education, Culture, Sports, Science and Technology (MEXT), Japan. Besides, the study was also supported in part by Kwang-Hua Education Fund of Tongji University, China.

References

ABAQUS. (2006), *Analysis user's manual-version 6.6*. ABAQUS, Inc., Pawtucket, R.I.

Chao, S.H., Khandelwal, K. and El-Tawil, S. (2006), "Ductile web fracture initiation in steel shear links", *J. Struct. Eng.*, ASCE, **132**(8), 1192-1200.

Divsalar, F., Wilson, Q. and Mathur S.B. (1988), "Low-cycle fatigue behavior of a structural steel", *Int. J. Pres. Ves. & Piping*, **33**, 301-315.

Dusicka, P., Itani, A.M. and Buckle, I.G. (2007), "Cyclic response of plate steels under large inelastic strains", *J. Constr. Steel Res.*, **63**, 156-164.

Ge, H.B., Kawahito, M. and Ohashi, M. (2007), "Ultimate strains of structural steels against ductile crack initiation", *Structural Eng./Earthquake Eng.*, JSCE, **24**(1), 13-22.

JSCE. (2000), *High performance steels for seismic design and high ductility structures*, Sub-Committee on Seismic Study of Steel Structures, Committee on Steel Structures, Japan.

Kanvinde, A.M. and Deierlein, G.G. (2008), "Validation of cyclic void growth model for fracture initiation in blunt notch and dogbone steel specimens", *J. Struct. Eng.*, ASCE, **134**(9), 1528-1537.
Krawinkler, H. and Zohrei, M. (1983), "Cumulative damage in steel structures subjected to earthquake ground motions", *Comput. Struct.*, **16**(1-4), 531-541.
Kuwamura, H. (1997), "Transition between fatigue and ductile fracture in steel", *J. Struct. Eng.*, ASCE, **123**(7), 864-870.
Li, D.M., Nam, W.J. and Lee, C.S. (1998), "An improvement on prediction of fatigue crack growth from low cycle fatigue properties", *Engineering Fracture Mechanics*, **60**(4), 397-406.
Liu, W.C., Liang, Z. and Lee, G.C. (2005a), "Low-cycle bending-fatigue strength of steel bars under random excitation. Part I: behavior", *J. Struct. Eng.*, ASCE, **131**(6), 913-918.
Liu, W.C., Liang, Z. and Lee, G.C. (2005b), "Low-cycle bending-fatigue strength of steel bars under random excitation. Part II: design considerations", *J. Struct. Eng.*, ASCE, **131**(6), 919-923.
McDaniel, C.C., Uang, C.M. and Seible, F. (2003), "Cyclic testing of built-up steel shear links for the new bay bridge", *J. Struct. Eng.*, ASCE, **129**(6), 801-809.
Sakano, M. and Wahab, M.A. (2001), "Extremely low cycle (ELC) fatigue cracking behaviour in steel bridge rigid frame piers", *J. Mater. Processing Technol.*, **118**, 36-39.

CC